CrossMark

Mechanical Properties of NiTi-Based Foam with High Porosity for Implant Applications

Ying Qiu[1,2] · Hao Yu[1] · Marcus L. Young[1]

Abstract In order to better understand NiTi-based shape memory alloy foams for implant applications, $Ni_{40}Ti_{50}Cu_{10}$ foams were heat treated and then deformed under incremental and cyclic compression loading. After heat treatment, the microstructure consists of a $(Ni,Cu)Ti$ matrix with small $(Ni,Cu)_4Ti_3$ precipitates and a large $Ti_2(Ni,Cu)$ secondary phase. The heat-treated $Ni_{40}Ti_{50}Cu_{10}$ foam exhibits a two-step transformation, involving $B19' \rightarrow B19$ and $B19 \rightarrow B2$ on heating and $B2 \rightarrow B19$ and $B19 \rightarrow B19'$ on cooling, respectively. One $Ni_{40}Ti_{50}Cu_{10}$ foam was compression loaded for 10 cycles at each subsequent strain level, i.e., 1, 2, 3, 4, 5, and 6 % strain. In each set of compressive stress–strain loops, the maximum stress level decreases due to plastic damage accumulation and/or retention of transformed martensite. Cross-sectional images from micro-computed tomography were collected during compression loading, which shows very uniform deformation without severe structural damage even up to 5 % strain. Localized deformation is visible at 6 % strain.

Keywords Stress–strain · Mechanical behavior · NiTi-based foam

✉ Marcus L. Young
marcus.young@unt.edu

1 Materials Science and Engineering, University of North Texas, Denton, USA

2 Mechanical and Energy Engineering, University of North Texas, Denton, USA

Introduction

NiTi-based shape memory alloys (SMAs) are excellent candidates for implant applications due to their unique shape memory effect and pseudoelasticity, good biocompatibility, high corrosion resistance, and relatively low stiffness as compared to other biomedical alloys [1–3]. By introducing porosity into NiTi-based SMAs, it is possible to tailor the stiffness and microstructure to more closely match that of bone as well as improve tissue and bone ingrowth [4, 5]. The addition of Cu, which substitutes for Ni in NiTi SMAs, such as $Ni_{40}Ti_{50}Cu_{10}$, improves the stability of the phase transformation temperatures responsible for the shape memory effect and pseudoelasticity (up to 8 % reversible strain) and narrows the phase transformation hysteresis [6–12]. Heat treatments can be used to enhance the mechanical properties, increase the phase transformation temperatures, and likely decrease Ni release, and thus, decrease toxic, allergic, and carcinogenic effects [13] by forming Ni_4Ti_3 precipitates, which also improve the phase transformation recovery.

Bricknell et al. [7] showed that the substitution of Cu for Ni in NiTi SMAs decreases the lattice distortion needed to form the martensite phase from the austenite phase, while still maintaining the ordered CsCl type structure at high temperature. Gil et al. [14, 15] showed that NiTiCu SMAs exhibit a much more narrow stress hysteresis, based on transformation stresses, as compared to binary NiTi SMAs. Fatigue testing of NiTiCu SMA actuator springs were conducted by Grossmann et al. [16, 17]. They reported that the functional fatigue resistance of NiTiCu SMAs is strongly improved by the addition of Cu. Sehitoglu et al. [18, 19] and Biscarini et al. [20] investigated the mechanical properties of NiTiCu single crystal SMAs under compression loading, and reported that the slip

resistance increases when Ni-rich precipitates are present. To date, the mechanical behavior of bulk NiTiCu SMA is well established [7, 14–19, 21–24]; however, few studies have focused on the effect of porosity on NiTiCu SMAs [25–28]. Goryczka et al. [26, 27] examined powder processing methods for producing homogenous NiTiCu SMAs. They found that porous NiTiCu SMAs show a similar martensite transformation behavior as compared to NiTiCu bulk materials. Porous NiTiCu SMAs can be optimized for implant applications due to the tunable stiffness, which can be tailored to match with the surrounding tissue or bone structure by controlling the porosity [9]. Young et al. [28] produced NiTiCu foams with 60 % porosity by casting a bulk NiTiCu SMA into SrF$_2$ salt preform and then dissolving away the SrF$_2$ salt preform with an acid solution. In this earlier study, the method for producing cast-replicated NiTiCu foams was presented as well as the microstructure and compression loading/unloading data for seven consecutive loops at body temperature (311 K) for a ∼60 % porous NiTiCu foam which was homogenized at 1173 K for 5 h. These foams exhibited 4 % recoverable strain and relatively low stiffness under single loading and unloading conditions at body temperature [28]. However, the mechanical behavior of these NiTiCu foams under cyclic loading conditions and the microstructural evolution after cyclic loading and unloading at room temperature have not been investigated. In the study presented here, a 76 % porous NiTiCu foam was produced from the same method as presented in Young et al. [28], resulting in a martensitic SMA at room temperature. This NiTiCu foam was additionally heat treated to obtain austenite at room temperature. The mechanical response and microstructural evolution of this austenitic NiTiCu foam was further examined at room temperature with micro-computed tomographic (μ-CT) imaging during incremental and cyclic in situ compression loading and unloading. The combination of mechanical loading and imaging allows for analysis of both the macroscopic and microscopic mechanical behavior of the NiTiCu foam.

Experimental

Ni$_{40}$Ti$_{50}$Cu$_{10}$ foams (referred to as NiTiCu foams throughout the paper) were prepared by a salt replication casting process [28, 29]. The process involved the following steps: (1) SrF$_2$ powders with 180 μm to 355 μm size were packed into an alumina crucible and sintering at 1673 K for 10 h under a vacuum with 10^{-4} Pa pressure, (2) a bulk NiTiCu SMA was then placed in an alumina crucible on top of an alumina spacer disc which was on top of the partially densified SrF$_2$ preform, (3) the crucible with the bulk NiTiCu SMA, alumina spacer disc, and the porous

SrF$_2$ preform was then heated under high vacuum to 1648 K. After holding at this temperature for 1 h, the chamber was then backfilled with Ar gas to a pressure of 1 atm, which forced the fully melted NiTiCu SMA into the porous SrF$_2$ preform, (4) the resulting NiTiCu/SrF$_2$ composite structure was then sectioned using an oil-cooled diamond wire saw (MTI Corporation, STX-202) into compression samples with approximate dimensions of $2.5 \times 2.5 \times 5.0$ mm^3, (5) the compression samples were ultrasonicated in an aqueous solution with 20 % nitric acid for 2 h in order to remove the space holder (SrF$_2$ preform), and (6) the NiTiCu compression samples were then sealed in evacuated quartz capsules and homogenized at 1173 K for 5 h, followed by water quenching, and then heat treated at 673 K for 8 h to improve the mechanical behavior by forming Ni$_4$Ti$_3$-like precipitates.

Differential scanning calorimetry (DSC) was conducted to study the phase transformation characteristics of the NiTiCu SMA foam using a Netzsch instrument (DSC 204 F1 Phoenix). DSC samples with a mass between 20 and 40 mg were individually sealed in cold-weldable, lidded aluminum crucibles, and subsequently heated and cooled from 203 to 373 K at a heating/cooling rate of 10 K/min. The DSC samples were held at the maximum and minimum temperature for 3 min to reach thermal equilibrium. Scanning electron microscopy (SEM) with energy dispersive spectroscopy (EDS) was performed on a FEI instrument (FEI quanta 200 ESEM). Density measurement of the NiTiCu SMA foam was carried out on a Micromeritics Pycnometer (Accupyc II 1340). The porosity (P) was calculated using the following equation:

$$P = \left(1 - \frac{\rho}{\rho_B}\right) \times 100 \%$$

where ρ is the measured density of NiTiCu foam and ρ_B is the density of bulk NiTiCu, 6.5 g/cm^3 [21].

A Skyscan1172 X-ray μ-CT scanner was used to perform combined cyclic compression testing and 3D X-ray tomography. The engineering strain measurements were based on the crosshead displacement, which was corrected and verified by testing a Teflon sample with similar dimensions as that of the NiTiCu foam compression sample. 3D X-ray tomographic images of the NiTiCu foam sample were collected before compression and at compression up to 1, 2, 3, 4, 5 and 6 % strain, where 10 loading/unloading cycles were performed at each strain level. X-ray μ-CT scanning was performed at a tube voltage of 100 kV and a tube current of 100 μA with an Al + Cu filter. X-ray radiographs were taken with an angular step of 0.4° and compiled to create a reconstructed 3D structure of the as-compressed NiTiCu foam sample. About 860 radiographs with a pixel size of 4.95 μm were obtained for each tomographic image. Image analysis

softwares (NRecon, CTvox, and Dataviewer) were used to perform the 3D reconstruction and analysis.

Results and Discussion

Figure 1a–c shows cross-sectional X-ray radiographs of the porous NiTiCu SMA foam in the x-, z-, and y-axes, respectively. Figure 1d shows the 3D reconstructed image of the porous NiTiCu SMA. These reconstructions were performed using NRecon software which confirms that the SrF_2 salt has been completely removed. As illustrated in Fig. 1a–d, the pore pattern and structure of the porous
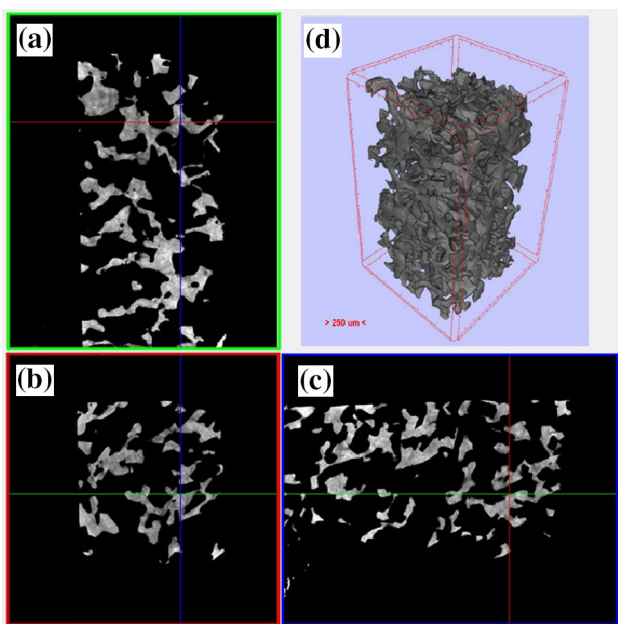
Fig. 1 Cross-sectional X-ray radiographs of the porous NiTiCu SMA foam for the **a** x- (*green box*), **b** z- (*red box*), and **c** y-axes (*blue box*) and **d** 3D reconstructed image of the porous NiTiCu SMA foam (Color figure online)
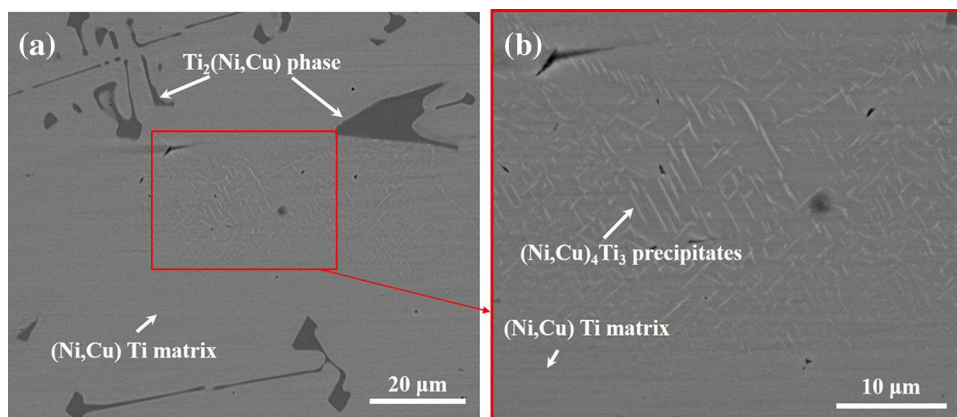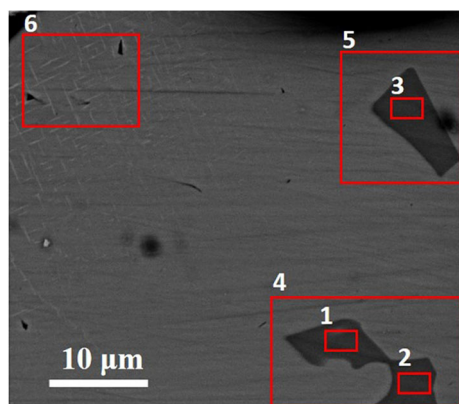
NiTiCu SMA foam sample after salt removal is readily visible and very uniform; however, most of the mass is centered on the nodes, which is a result of the geometry of the SrF_2 particles and the salt replication processing. The density of the porous NiTiCu foam sample was measured to be 1.55 g/cm^3, corresponding to a porosity of about 76.2 %. This high porosity is also verified by the 3D reconstructed image of the porous NiTiCu foam (Fig. 1d). Similar structures have been observed in other metal foams prepared by this method [28–30]. As indicated in Fig. 1a–c, the foam is fully interconnected, which is favorable to accommodate uniform compression deformation.

As illustrated in Fig. 2a, b, SEM images of the NiTiCu foam after heat treatment reveal a (Ni,Cu)Ti matrix with small $(Ni,Cu)_4Ti_3$ precipitates and a large dendritic Ti_2 (Ni,Cu) secondary phase. Like the Ti_2Ni phase in NiTi binary SMAs [23, 28], the $Ti_2(Ni,Cu)$ phase is brittle and thus detrimental to the shape memory effect and mechanical behavior [28]. This phase forms in a peritectic reaction in the NiTi matrix during the melting process (1375 °C, 1 h, Ar gas) and is commonly stabilized by interstitial oxygen atoms [28, 31]. $(Ni,Cu)_4Ti_3$ precipitates are the lenticular particles, which are the typical four variant Ni_4 Ti_3 precipitates morphology [32], shown distributed in Fig. 2b. The $(Ni,Cu)_4Ti_3$ phase corresponds to Ni_4Ti_3 phase in binary NiTi SMAs and forms in the NiTi matrix during the heat treatment process (400 °C, 8 h). The formation of $Ti_2(Ni,Cu)$ and $(Ni,Cu)_4Ti_3$ phase affects the Ni content of the (Ni,Cu)Ti matrix, which in turn has an influence on the martensite transformation temperatures [33]. As shown in the SEM image in Fig. 3, EDS measurements were collected from 6 different regions. The EDS data for Fig. 3 are shown in Table 1, where the compositions of the various phases can be seen. The addition of Cu distorts the ratio of Ni to Ti, however, it is not clear what the role of Cu is and how it affects the formation of $Ti_2(Ni,Cu)$ and $(Ni,Cu)_4Ti_3$ phases in this alloy.

Fig. 2 a SEM image and **b** detailed view of the same SEM image of NiTiCu SMA foam after heat treatment

As indicated in Fig. 4, the DSC curves for the heat-treated NiTiCu foam exhibit a two-step phase transformation below room temperature (298 K), which corresponds to B19′ → B19 and B19 → B2 on heating and B2 → B19 and B19 → B19′ on cooling, respectively, and indicate that the foam is fully austenitic at room temperature (298 K). The bulk NiTiCu SMA material exhibits a two-step transformation as well, but is fully austenitic above ∼348 K. A similar NiTiCu foam with lower porosity (∼60 %) and no heat treatment is fully austenitic at body temperature (311 K) [28]. The heat treatment (673 K for 8 h) performed in this study was effective at lowering the transformation temperatures such that the NiTiCu foam is fully austenitic at room temperature. This additional heat treatment should result in the formation of $(Ni,Cu)_4Ti_3$ precipitates and this is confirmed in the SEM images shown in Fig. 2b, where more $(Ni,Cu)_4Ti_3$ precipitates are observed as compared to those observed in [28] without this heat treatment. If more $(Ni,Cu)_4Ti_3$ precipitates formed, one would expect to observe an increase in the transformation temperatures, as the $(Ni,Cu)Ti$ matrix would be depleted of Ni [31]. However, the transformation temperatures are observed to decrease instead and a two-step transformation is observed rather than a 1-step transformation. It is unclear why this decrease occurred and why there is now a two-step transformation as opposed to a one-

step transformation after heat treatment. Transformation temperatures can be lowered by precipitating more Ti_2(Ni,Cu), but this should not occur, because Ti_2(Ni,Cu) is not likely to precipitate at the lower temperature heat treatment. It was not possible to determine if more Ti_2(Ni,Cu) was precipitated. Further complicating the situation is the fact that Ti_2(Ni,Cu) precipitates can be stabilized by forming the Ti_4(Ni,Cu)$_2$O or Ti_2NiO_x phase [28, 31], although this oxidation should not affect the transformation temperatures as the matrix composition would not have changed with oxidation. This result is difficult to explain but may be due to heterogeneity from processing and non-equilibrium cooling conditions in the NiTiCu foam where more Ti_2(Ni,Cu) could have formed and thus lowered the transformation temperatures.

As compared to the bulk material, the transformation temperatures are lower due to the decrease in Ti (or alternatively the increase in Ni) in the $(Ni,Cu)Ti$ matrix. This difference in transformation temperatures between the porous foam and the bulk material is the result of the formation of Ti_2(Ni,Cu) and $(Ni,Cu)_4Ti_3$ precipitates during processing and heat treatment. Ti_2(Ni,Cu) phase increases the Ni content in the matrix by pulling Ti out of the matrix, while $(Ni,Cu)_4Ti_3$ phase is apt to decrease Ni content by pulling Ni out of the matrix. The formation of these two phases affects the transformation temperatures by changing the matrix composition [31]. As compared to our previous NiTiCu foam [28] which was processed identically except that it was not heat treated after homogenization, the austenite start temperature (∼293 K) for the NiTiCu foam presented here is about 6 K lower than that previously reported value. As a result, the NiTiCu foam presented here is austenitic at room temperature and has slightly more $(Ni,Cu)_4Ti_3$ precipitates, which are also observable in Fig. 2b as compared to Fig. 4b in Young et al. [28].

The compressive loading and unloading curves for the NiTiCu SMA foam and the corresponding 3D reconstructed images are shown in Fig. 5. There is no apparent stress plateau in any of the stress–strain curves even when the strain is as high as 6 %, which is slightly different from the mechanical behavior of bulk NiTiCu SMA materials [18]. This difference is likely due to the high porosity,

Fig. 3 SEM images of NiTiCu SMA foam after heat treatment (red boxes 1, 2, 3, 4, 5, and 6 corresponding to the regions in Table 1) (Color figure online)

Table 1 Phases identified by EDS analysis

Region	Ti (at.%)	Ni (at.%)	Cu (at.%)	Possible phase
1	62.26	33.30	4.44	Ti_2(Ni,Cu) phase
2	62.37	33.60	4.03	Ti_2(Ni,Cu) phase
3	64.24	31.81	3.95	Ti_2(Ni,Cu) phase
4	47.22	43.00	9.78	$(Ni,Cu)Ti$ matrix and Ti_2(Ni,Cu) phase
5	47.79	42.94	9.26	$(Ni,Cu)Ti$ matrix and Ti_2(Ni,Cu) phase
6	46.74	38.21	15.05	$(Ni,Cu)Ti$ matrix and $(Ni,Cu)_4Ti_3$ precipitates

which results in the fracture of the thin struts or weak nodes before the critical transformation stress is reached [28]. For the first strain level, the sample was loaded to 1 % strain and then unloaded to obtain one loop; the same operation was repeated 10 times. This data is not presented since it has considerable error associated with it due to the large step size (0.01 mm) of the loading stage and at that level it is only possible to collect at maximum 5 data points. After the specimen was compressed to 2, 3, 4 and 5 % for 10 times, all the strains are fully recoverable in the range of the detector capacity of the load frame in μ-CT. For 6 % compression, about 1.5 % strain did not recover after unloading. As shown in the 3D reconstruction images in Fig. 5, the majority of the structural features remain intact after multiple compression cycles. In general, the loops decrease in maximum stress with each subsequent

compression cycle. The maximum stress obtained is about 4 MPa for 2 % compression and that value increases to 8 MPa for all subsequent compression strains (e.g., 3, 4, 5, and 6 % strain). Therefore, the slope of the stress–strain curve decreases or in other words the macroscopic elastic modulus softens, because more thin struts are involved in the compression and are damaged as the strain increases, as shown in Figs. 5 and 6. The NiTiCu SMA foam appears fully elastic up to 5 % strain macroscopically. This elasticity results from either a composite effect and/or is associated with the pseudoelastic effect. However, the onset of localized damage can be seen at 3 % strain, which is likely due to the retention of the displacement or macroscopic damage at the top of the NiTiCu SMA sample, as observed microscopically in Figs. 5 and 6 using μ-CT during in situ compression loading.

In order to examine the compression behavior internally within the NiTiCu SMA foam, a 2D cross-sectional image from each 3D reconstruction model which is parallel to the loading direction was examined at the end of each strain level after 10 cycles, as shown in Fig. 6. The majority of internal struts and nodes remain fully intact during compression cycling, while the height of the sample slightly decreases in the loading direction, which is expected after compression due to some localized plastic deformation. Some portions of the NiTiCu SMA foam moved down in the loading direction as the strain increased, (red ellipse labeled A in Fig. 6). This deviation in position is the direct result of damage accumulation. While some localized catastrophic damage near the top (blue box labeled B in Fig. 6) becomes visible, further visual inspection of these images reveals that a boundary can be defined as indicated by the red line in Fig. 6, below which structural
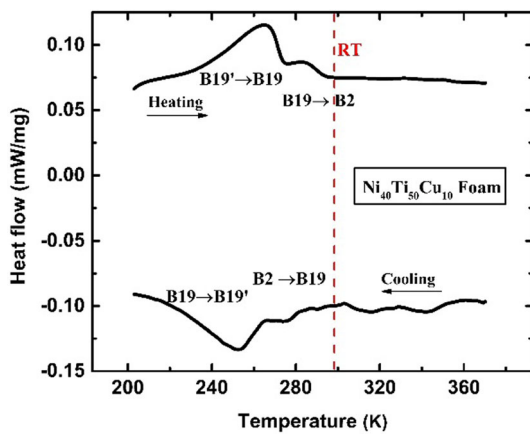

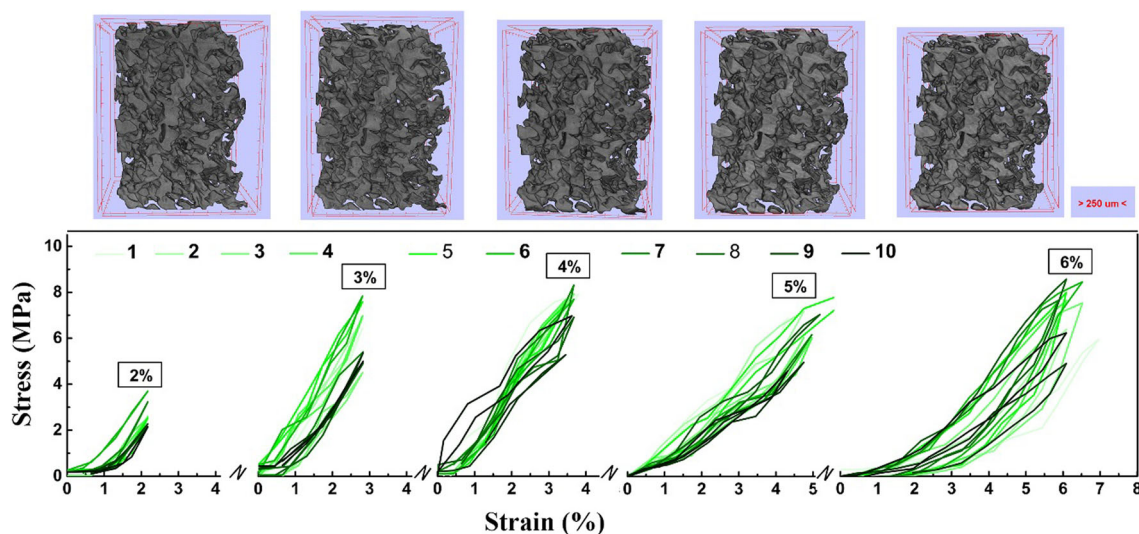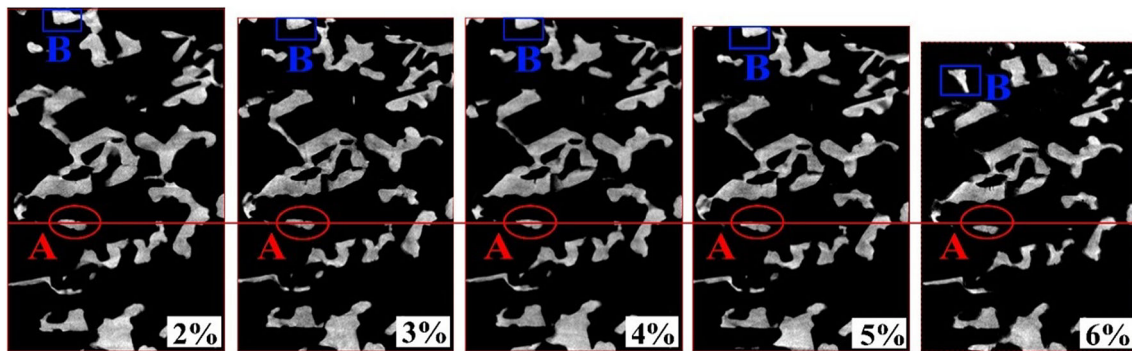**Fig. 4** DSC curves for the heat-treated NiTiCu SMA foam

Fig. 5 2D cross-sectional images of the NiTiCu SMA foam parallel to the loading direction after compression to 2, 3, 4, 5, and 6 % strain, respectively

Fig. 6 Stress–strain curves from compression cycling for the NiTiCu SMA foam and corresponding 3D reconstructed X-ray μ-CT images of the NiTiCu SMA foam after compression to 2, 3, 4, 5, and 6 % strain, respectively

deformation is not apparent as compared with the region above the red line. This result is probably due to the relatively large struts and nodes which are interconnected and help to decentralize the external stress, thus preventing large plastic deformation or structural damage, or in other words, the stress remains localized during compression. However, the outer struts that lack interconnectivity in at least one direction tend to deform first, especially the thinner and, therefore weaker struts. As shown Fig. 5, the stress level remains constant at about 8 MPa when the strain increases from 2 to 6 % and this behavior is likely due to these weaker struts deforming in compression. At 6 % strain, plastic deformation is apparent in both the stress–strain curves (Fig. 5) where some unrecoverable residual strains are present, and some large scale macroscopic visual damage is observed in Fig. 6, blue box labeled B.

Conclusions

In the present research, $Ni_{40}Ti_{50}Cu_{10}$ SMA foams were heat treated and then deformed under incremental and cyclic compression loading conditions. The conclusions are as follows:

1. The SrF_2 space holder was removed by ultrasonic vibration in a 20 % HNO_3 aqueous solution for 2 h to create the porous NiTiCu SMA foam. After heat treatment, the NiTiCu foam consisted of a (Ni,Cu)Ti matrix with small $(Ni,Cu)_4Ti_3$ precipitates and a large dendritic $Ti_2(Ni,Cu)$ secondary phase. The NiTiCu SMA foam has a density of 1.55 g/cm^3 and a porosity of 76.2 %, which is higher than a NiTiCu SMA foam previously studied, likely due to a higher amount of metal dissolution during salt removal.

2. The $Ni_{40}Ti_{50}Cu_{10}$ SMA foam exhibits a two-step phase transformation, which corresponds to $B19' \rightarrow B19$ and $B19 \rightarrow B2$ on heating and $B2 \rightarrow B19$ and $B19 \rightarrow B19'$ on cooling. The NiTiCu SMA foam here is austenitic at room temperature, with an austenite start temperature ($\sim$293 K). While $(Ni,Cu)_4Ti_3$ precipitates are more abundant after heat treatment, the transformation temperatures are lower, which is unexpected. This result may be due to heterogeneity from processing and non-equilibrium cooling conditions in the NiTiCu foam where more $Ti_2(Ni,Cu)$ could have formed and thus lowered the transformation temperatures. The transformation temperatures are also about 50 K lower than bulk NiTiCu SMA materials.

3. The compressive stress–strain curves of the porous $Ni_{40}Ti_{50}Cu_{10}$ SMA foam do not exhibit an apparent stress plateau even when the strain is as high as 6 %. Localized deformation results in relatively constant stress level when the strain increases from 2 to 6 % and this response is either a composite effect and/or is associated with the pseudoelastic effect. Beyond 6 % strain, both unrecoverable strains can be seen in the stress–strain curves as well as in the X-ray μ-CT tomographic images, which is associated with plastic deformation.

References

1. Andani MT, Shayesteh Moghaddam N, Haberland C, Dean D, Miller MJ, Elahinia M (2014) Metals for bone implants. Part 1. Powder metallurgy and implant rendering. Acta Biomater 10:4058. doi:10.1016/j.actbio.2014.06.025

2. Li B-Y, Rong L-J, Li Y-Y (1998) Porous NiTi alloy prepared from elemental powder sintering. J Mater Res 13:2847

3. Fischer H, Vogel B, Welle A (2004) Applications of shape memory alloys in medical instruments. Minim Invasive Ther Allied Technol 13:248

4. Grummon DS, Shaw JA, Gremillet A (2003) Low-density open-cell foams in the NiTi system. Appl Phys Lett 82:2727. doi:10.1063/1.1569036

5. Greiner C, Oppenheimer SM, Dunand DC (2005) High strength, low stiffness, porous NiTi with superelastic properties. Acta Biomater 1:705. doi:10.1016/j.actbio.2005.07.005

6. Nam TH, Saburi T, Nakata Y, Ki Shimizu (1990) Shape memory characteristics and lattice deformation in Ti-Ni-Cu alloys. Mater Trans JIM 31:1050

7. Bricknell R, Melton K, Mercier O (1979) The structure of NiTiCu shape memory alloys. Metall Trans A 10:693

8. Arciniegas M, Aparicio C, Manero JM, Gil FJ (2007) Low elastic modulus metals for joint prosthesis: tantalum and nickel–titanium foams. J Eur Ceram Soc 27:3391. doi:10.1016/j.jeurceramsoc.2007.02.184

9. Bansiddhi A, Sargeant TD, Stupp SI, Dunand DC (2008) Porous NiTi for bone implants: a review. Acta Biomater 4:773. doi:10.1016/j.actbio.2008.02.009

10. Barrabés M, Sevilla P, Planell JA, Gil FJ (2008) Mechanical properties of nickel–titanium foams for reconstructive orthopaedics. Mater Sci Eng C 28:23. doi:10.1016/j.msec.2007.02.001

11. Scalzo O, Turenne S, Gauthier M, Brailovski V (2009) Mechanical and microstructural characterization of porous NiTi shape memory alloys. Metall Mater Trans A 40:2061. doi:10.1007/s11661-009-9906-1

12. Kockar B, Ozcan H, Cakmak S (2013) Shape memory behavior of Ni-rich NiTi foam with different porosity percentages. J Intell Mater Syst Struct 24:1131. doi:10.1177/1045389x12469450

13. Chen M-C, Wu S-K (2009) Surface analyses and biocompatibility study of 500 & #xB0;C oxidized Ni50Ti50 and Ni40Ti50Cu10 shape memory alloys. Surf Coat Technol 203:1715. doi:10.1016/j.surfcoat.2009.01.012

14. Gil F, Solano E, Pena J, Engel E, Mendoza A, Planell J (2004) Microstructural, mechanical and citotoxity evaluation of different NiTi and NiTiCu shape memory alloys. J Mater Sci Mater Med 15:1181

15. Gil F, Planell J (1999) Thermal efficiencies of NiTiCu shape memory alloys. Thermochim Acta 327:151

16. Grossmann C, Frenzel J, Sampath V et al (2008) Processing and property assessment of NiTi and NiTiCu shape memory actuator springs. Materialwiss Werkstofftech 39:499. doi:10.1002/mawe.200800271

17. Grossmann C, Frenzel J, Sampath V, Depka T, Eggeler G (2009) Elementary transformation and deformation processes and the cyclic stability of NiTi and NiTiCu shape memory spring actuators. Metall Mater Trans A 40:2530

18. Sehitoglu H, Karaman I, Zhang X et al (2001) Deformation of NiTiCu shape memory single crystals in compression. Metall Mater Trans A 32:477

19. Sehitoglu H, Karaman I, Zhang X, Viswanath A, Chumlyakov Y, Maier H (2001) Strain–temperature behavior of NiTiCu shape memory single crystals. Acta Mater 49:3621

20. Biscarini A, Coluzzi B, Mazzolai G, Tuissi A, Mazzolai FM (2003) Extraordinary high damping of hydrogen-doped NiTi and NiTiCu shape memory alloys. J Alloys Compd 355:52. doi:10.1016/s0925-8388(03)00267-6

21. Frantz-Rodriguez N, Bosseboeuf A, Dufour-Gergam E et al (2000) Composition and structure of NiTiCu shape memory thin films. J Micromech Microeng 10:147

22. Kotil T, Sehitoglu H, Maier HJ, Chumlyakov YI (2003) Transformation and detwinning induced electrical resistance variations in NiTiCu. Mater Sci Eng A 359:280. doi:10.1016/s0921-5093(03)00365-4

23. Michaud V (2004) Can shape memory alloy composites be smart? Scripta Mater 50:249. doi:10.1016/j.scriptamat.2003.09.016

24. Miller DA, Lagoudas DC (2000) Thermomechanical characterization of NiTiCu and NiTi SMA actuators: influence of plastic strains. Smart Mater Struct 9:640

25. Atiyah AA, Ali A-RKA, Dawood NM (2015) Characterization of NiTi and NiTiCu porous shape memory alloys prepared by powder metallurgy (Part I). Arab J Sci Eng 40(3):901–913

26. Goryczka T, Van Humbeeck J (2006) Characterization of a NiTiCu shape memory alloy produced by powder technology. J Achiev Mater Manuf Eng 17(1–2):65–68

27. Goryczka T, Van Humbeeck J (2008) NiTiCu shape memory alloy produced by powder technology. J Alloys Compd 456:194. doi:10.1016/j.jallcom.2007.02.094

28. Young ML, DeFouw JD, Frenzel J, Dunand DC (2012) Cast-replicated NiTiCu foams with superelastic properties. Metall Mater Trans A 43:2939. doi:10.1007/s11661-011-1060-x

29. Brothers AH, Scheunemann R, DeFouw JD, Dunand DC (2005) Processing and structure of open-celled amorphous metal foams. Scripta Mater 52:335. doi:10.1016/j.scriptamat.2004.10.002

30. San Marchi C, Mortensen A (2001) Deformation of open-cell aluminum foam. Acta Mater 49:3959

31. Frenzel J, George EP, Dlouhy A, Somsen C, Wagner MFX, Eggeler G (2010) Influence of Ni on martensitic phase transformations in NiTi shape memory alloys. Acta Mater 58:3444. doi:10.1016/j.actamat.2010.02.019

32. Michutta J, Somsen C, Yawny A, Dlouhy A, Eggeler G (2006) Elementary martensitic transformation processes in Ni-rich NiTi single crystals with Ni_4Ti_3 precipitates. Acta Mater 54:3525

33. Khalil-Allafi J, Dlouhy A, Eggeler G (2002) Ni_4Ti_3-precipitation during aging of NiTi shape memory alloys and its influence on martensitic phase transformations. Acta Mater 50:4255